Modification of swept-wing tip vortex with nature-inspired, serrated leading edge

Alden Midmer* and Christoph Brücker†
City, University of London, London , EC1V 0HB

Owls have evolved unique wing features that enable silent flight, a crucial adaptation for their nocturnal hunting strategy. This study investigates the role of leading edge combs, also known as serrations or barbs, in reducing noise emissions and enhancing aerodynamic performance. Previous research has demonstrated the positive effects of serrations on both noise suppression and aerodynamic efficiency on rectangular wings. However, the aerodynamic mechanism by which serrations contribute to noise suppression on swept wings remains unexplored. We speculate herein that this is specifically affecting the tip vortex noise at varying angles of attack, inspired from animal studies with removed serrations. Experiments using particle image velocimetry (PIV) and flow visualization techniques are employed and show the flow turning induced by serrations and its subsequent effect on tip vortex formation, which results in lower vortex strength and core size, linked towards reduced vortex-induced noise emission. The results demonstrate the passive and three-dimensional flow control dependent on inflow conditions and offer an insight into the mechanism by which serrations contribute to silent flight, particularly during the final stages of hunting. It is also suggested that the serrations work in similar fashion to other swept wing flow control devices in attenuating the spanwise velocity component and increasing stall AoA.

I. Nomenclature

c	=	chord length
C_l	=	Lift coefficient
H	=	Serration height
L	=	Serration length
Re_c	=	Chord based Reynolds number
Re_s	=	Serration based Reynolds number
SAR	=	Semi-Aspect Ratio
U_{inf}	=	Mean flow velocity
α, AoA	=	Angle of attack
β	=	Sweep angle
λ	=	Serration wavelength

II. Introduction

Owls rely on sound to hunt and have therefore developed adaptations to reduce self noise and enable silent flight. This also has the added benefit of making it more difficult for the prey to detect the owl. There are three main proposed features of an owl's wing that suppress noise levels: a velvety suction side wing surface, a flexible trailing edge fringe and, of most interest to this study, the leading edge comb [1, 2](also known as serrations or barbs). The leading edge comb has been studied with regard to noise suppression and aerodynamic performance enhancement [3, 4] with positive results in both cases. The serrations were shown to be able to delay the onset of stall and reduce the noise emission by suppressing incoming turbulence impacting the leading edge. Both are thought to be partly due to the flow turning effect first highlighted by [5] and depicted in fig. 1. However, the performance of the leading edge serrations are very sensitive to the geometry of the serrations themselves and the angle of attack of the airfoil.

*PhD Student, Department of Aeronautical Engineering, alden.midmer@city.ac.uk
†Sir Richard Olver BAE Systems Chair in Aeronautical Engineering, Department of Aeronautical Engineering, christoph.breucker@city.ac.uk.

Acoustic measurements on flying owls ([3, 6–10]) and owl wings indicated that the serrations are able to reduce flight-noise. A comparison between noise production in barn-owl flight with serrations and after the serrations have been removed was performed by [7]. It was found that serrations reduce noise before landing at high angles of attack but not during gliding flight. [3, 10] suggest the reduction in flight noise at higher AoA is related to a larger contribution of the tip vortex noise to the overall noise generated during the flaring maneuver, suggesting that serrations could be helpful in reducing the tip vortex noise at large angles of attack. What is missing in research so far is the further understanding on the influence of the serrations on the tip vortex development, specifically with varying angles of attack.

Serrations can also be compared to other flow control devices specifically for swept wings. These can either be passive or active systems such as wing fences or vortex generating jets. The main purpose of these devices are to inhibit the spanwise velocity component, delay separation and subsequently maintain control surface effectiveness [11]. The passive systems often provide some form of physical barrier to prevent cross flow and generate vortices near the leading edge, often at the expense of increased drag [12]. Whereas the vortex injection systems blow jets tangential to the wings surface and orientated towards the wing root. These devices can provide more favorable aerodynamic performance (increased C_l and stall angle depending on configuration) but are more difficult to implement onto a wing [13]. We further test herein the serrations effect on the spanwise velocity component and subsequent development of the tip vortex which is not only a source of noise but also contributes to aerodynamic inefficiency.

The paper is formatted as follows: initially an overview of the serration and wing model is given, including the geometry and characteristics of the serrations being tested and followed by the experimental setups for each of the testing configurations and the processing method. In section VI the results are shown and discussed, starting with the effects of the barbs on the freestream, followed by the effects of the serrations with increased angle of attack. The serrations are then applied to airfoils of different sweep angles and the effects on the vortex development are then compared to identical airfoils without serrations attached.

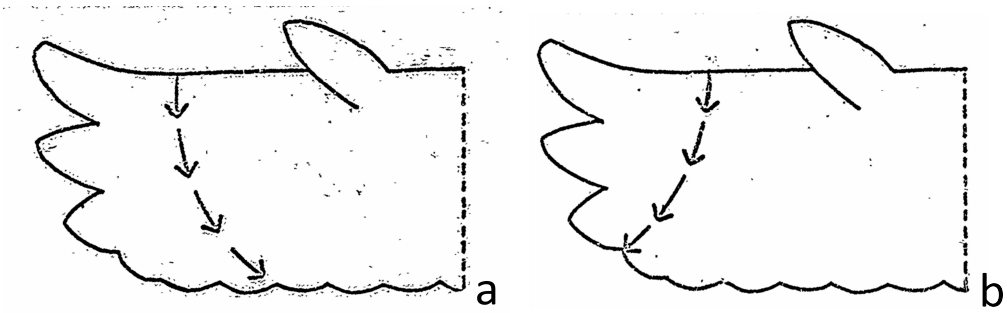

Fig. 1 Flow turning effect of owl serrations at low (a) and high (b) AoA, modified from [5].

III. Serration geometry

The physical model used herein is the same as that introduced by [14] (where a thorough description on the development of the model are given) and is 4× larger in scale compared to the barbs found in nature. Therefore typical heights of the barbs of $h = 1mm$ in nature result into structures with a height $H = 4mm$ in the model.[15, 16]). We attached the base of the comb to a custom airfoil and for the analysis of the flow turning effect, a larger 20× model was instead used. The idealized model has uniform barb dimensions, geometries and a constant wavelength of a $\lambda = 0.5H$ (fig. 2a,c). An important feature of the serrations are the tapering of the barbs towards the tip, resulting in an also increasing free space between the barbs towards the tip (fig. 2c). Another feature is the twist (in streamwise direction; x), where the barbs have zero twist at the tip (in line with the flow) and maximum twist at the root ([17]), in favor of inboard flow turning; this results in reducing profile area with height (fig. 2a).

IV. Wing models

The airfoil used was a custom designed symmetric profile with a flat midsection, rounded leading edge and tapered trailing edge. The flat section was from $x/c = 0.15 - 0.75$ and the maximum thickness of the airfoil was 4.5%. This airfoil was used to make it easier to align the laser and test the flow turning effect in the chord-parallel measurements (see fig. 4b), along with having a similar thickness to serration height ratio found on owl wings.

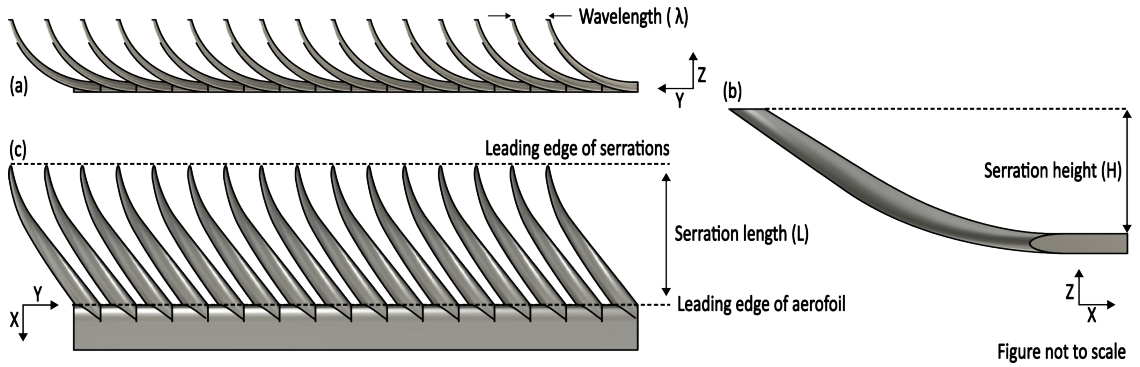

Fig. 2 Orientation of the idealized serration model, showing the yaw, inclination (pitch), varying twist and thickness of each barb. a) Front-view, looking parallel to the flow. b) Side-view of the serrations (enlarged). c) Top-view of the serrations, looking normal to the plate surface. (geometry re-illustrated from [14])

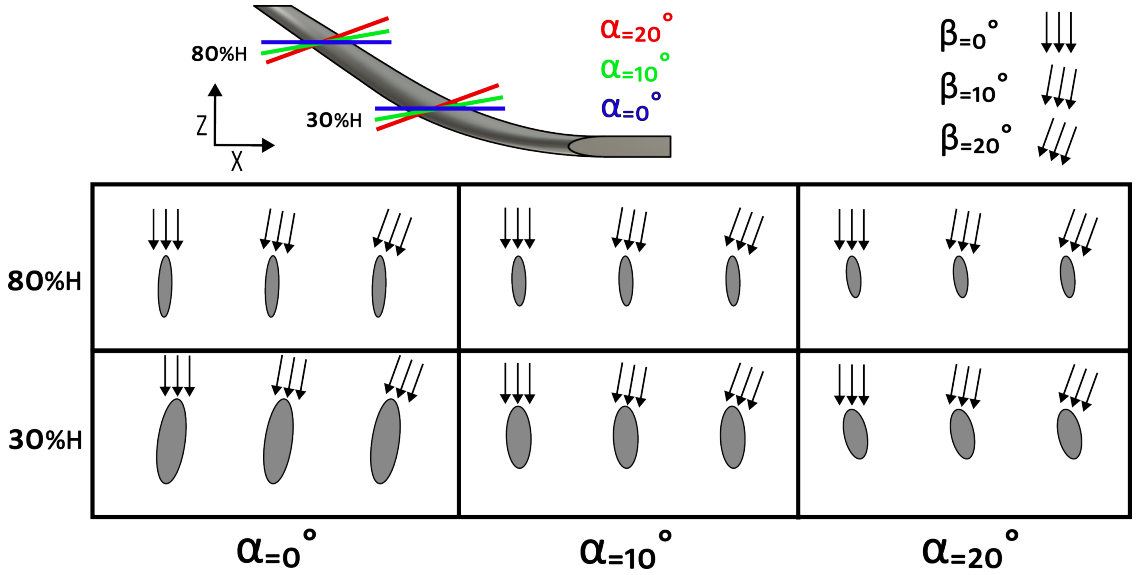

Fig. 3 Cross-section view of the serrations at varying heights and angles of attack.

Two wing models were used with varying sweep, 10° and 20°, which are typical of the sweep angle of barn owls during different phases of flight [14]. In each case the Semi-Aspect Ratio of the wing remained consistent ($SAR = 1.5$). At the front of the wing section was a slot which allowed for the interchange of leading edge; one rounded, reference leading edge and one with serrations. The wing was furthered attached with an end plate to minimize the surface effects of the water tunnel.

V. Methodology

In this study we make use of the fundamental aspects of similitude in fluid mechanics, which means that the flow features and streamlines are identical for different scaling factors of the geometry as long as the non-dimensional flow parameters such as the Reynolds number are similar [18]. For low Mach numbers (Ma ≤ 0.1) the flow is in the incompressible range and one can therefore use studies in a water-tunnel to analyze the streamlines around a wing similar to those experienced in air. Herein, for the reason of better experimental conditions and limitations of current printing resolution, we used a large-scale model of the barbs, which is then studied in a water tunnel with good optical conditions for high-quality flow mapping using PIV [19]. A 4× scaled model of the reconstructed barbs affixed to wings of varying sweep was tested in the CHB water tunnel at City, University of London, at a serration chord based Reynolds-number of $Re_s = 150$ (equating to a chord based Reynolds number of $80,000$) which is typical for gliding

flight conditions of owls in air (Re_c = 50000 − 10000, [20]). Further testing of the serrations at a 20× scale was also done at the same Re_s = 150 for a more detailed analysis of the serration/ fluid interaction.

The tunnel was a closed loop with a honeycomb mesh located upstream of the test section and baffle foam located downstream. Running the length of the test section was a traverse, to which the wing models were mounted to. The test section, with transparent walls, had dimensions of 0.4 m width, 0.5 m depth and 1.2 m length. The serration model was placed in the test section so that the spanwise axis of the comb is aligned with the vertical axis and with the serrations facing the flow, see fig. 4.

A. PIV setup and camera arrangement

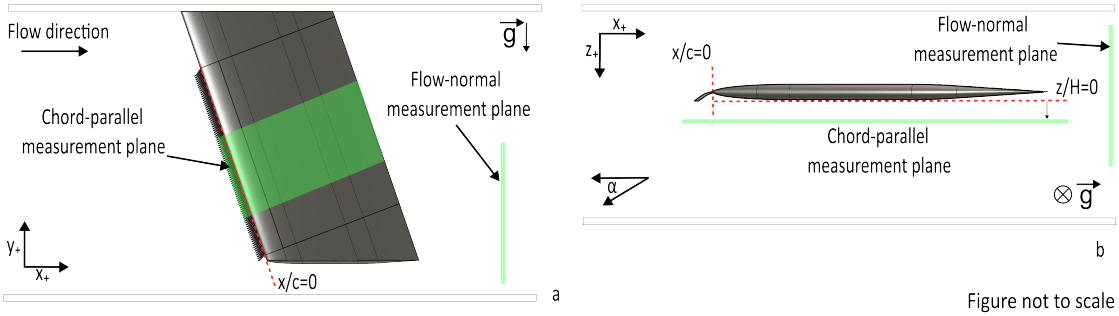

Fig. 4 Experimental setup for the chord and flow normal measurement planes.

1. Wing tip, vortex testing

In the flow normal measurements a 5 Watt continuous wave laser (Dantec Dynamics RayPower, 532 nm wavelength) equipped with light-sheet optics was positioned perpendicular to the mean flow. The light sheet was of 5 mm nominal thickness which meant each particle remained within the lighsheet long enough to record the secondary flow structures. A Phantom Miro M310 high speed camera (1280 × 800 pixel sensor size) equipped with a Tokina 100 mm macro lens was used to capture the flow. Due to the relatively low velocities used the frame rate was set to 200fps ($\Delta t = \frac{1}{200} s$) with exposure times of 4500 µs. A 45° mirror was placed in the flow channel downstream, the camera was then focused onto the light sheet via the mirror. Throughout the tests the light sheet remained stationary and between tests the wing was traversed along the tunnel to obtain the desired x/c location. The downstream measurement planes were at x/c = 1, 1.5, 2 (fig. 4c). For the seeding plastic particles, of approximate diameter 20 µm, were used as the seeding and placed into, and allowed to circulate around, the tunnel prior to testing.

2. 20× scale model testing

For the measurement series with the 20× scale model the same light sheet as above was re-positioned parallel to the bulk flow via a mirror underneath the test section. The mirror was also fitted to a traverse so the light sheet could be moved along the height of the serrations, allowing for the measurement of the flow in different cross-sections along the barb height. The serration height ranged from 0%H at the root to 100%H at the tip. The tests were conducted at two barb heights of 30%H and 80%H. As the Reynolds number remained consistent with the 4× scale model the incoming velocity was reduced and subsequently the frame rate was also reduced to 60fps.

B. Processing

Processing of the captured image sequences, with 1600 images per test (500 images for the 20× scale model), was done via PIVlab ([21]) followed by further post-processing of the plots on *tecplot*. The background mean intensity, determined over the entire frame and time series, was first subtracted from each of the images before being processed. Each consecutive image-pair of the sequence was processed with the method of digital cross-correlation (correlating frame n with frame n+1) in a two-pass iteration with 50% overlap of the interrogation window (the window size remained constant with $32px \times 32px$). Image masking was applied for regions, where the serrations enter the light-sheet or in

regions of shadows cast by the serrations. The resulting 1599 velocity fields (499 for the 20× scale model) were then refined via a local median-filter to remove erroneous vectors.

The vector field was then exported to *tecplot* where the Q-criterion were calculated (with the *pytecplot* function) and then normalized with respect to U_{inf} and c.

VI. Results

A. Flow turning effect

Initially the serrations were tested without the presence of a pressure gradient (attached to a flat plate and at 0°) and with the larger, 20× scale model. This was to analyse the flow turning effect and, to be able to do so at different serration heights which could not be achieved with the 4× scale model. Measurements were taken at two serration heights of 30% and 80% at AoAs from 0° to 30° at intervals of 5°.

1. Reference cases

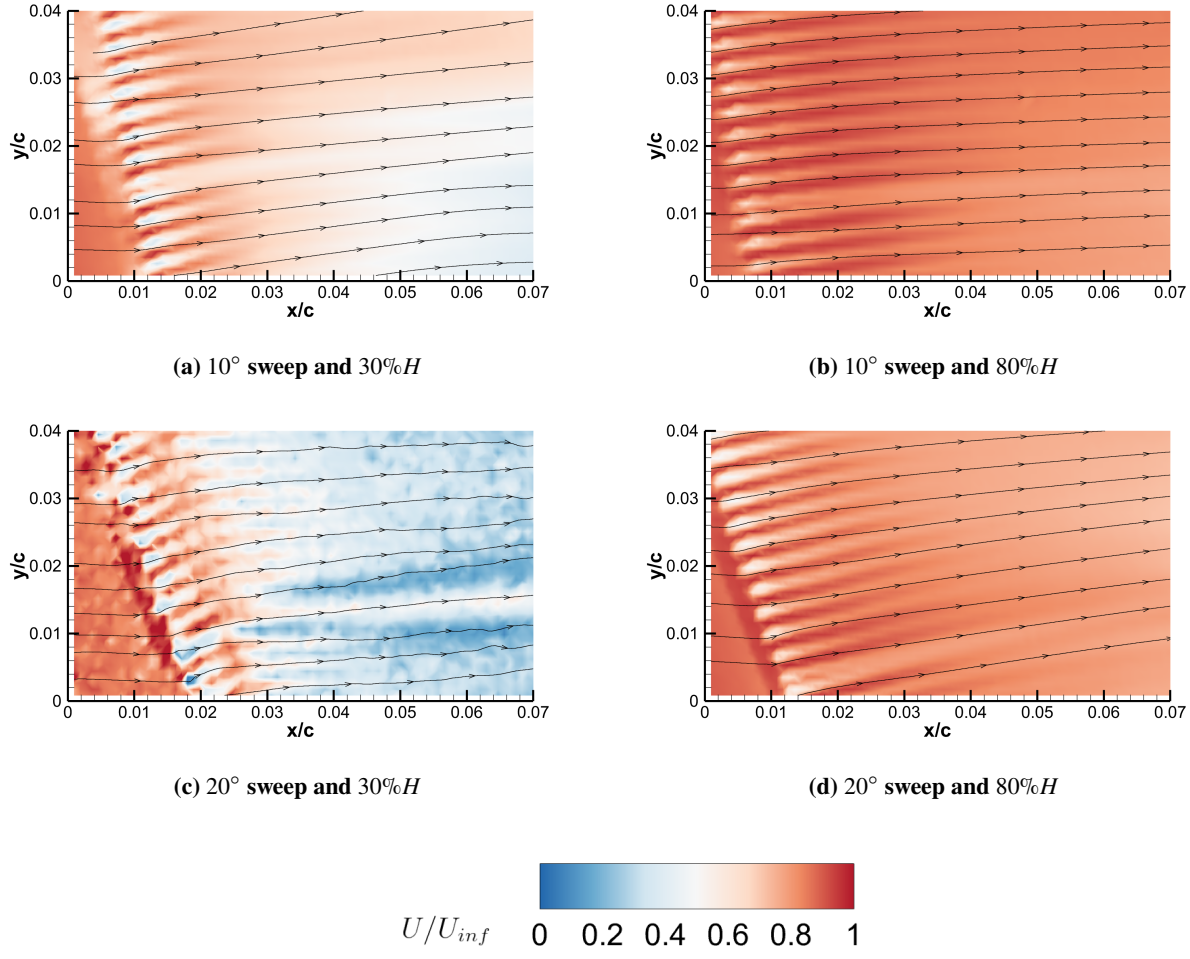

(a) 10° **sweep and** 30%H

(b) 10° **sweep and** 80%H

(c) 20° **sweep and** 30%H

(d) 20° **sweep and** 80%H

Fig. 5 Serration reference case velocity magnitude contours with overlaid streamlines at 0° **AoA and** $Re_s = 80,000$ **at different sweep angles.**

Figure 5 shows the reference case of the serrations with 10° and 20° sweep at two serration heights, the flow turning regardless of sweep angle is broadly consistent - the flow is turned inboard (y+). However as the cross sectional profiles

at both heights are similar (3) for the $\alpha = 0°$ the slight difference in flow turning is determined by the sweep angle of the serrations.

A significant deviation from the mean flow is also observed between the different sweep angles and serration heights. At both sweep angles a greater reduction in velocity occurs at the lower serration height, due to the increased frontal area towards the root of the barbs. The increase in frontal area is further exacerbated with 20° sweep, resulting in a velocity deficit of up to 80%. This can again be interpreted from the cross section slices (fig. 3) in which, due to the sweep angle, the incoming flow is presented with a larger portion of the barb inner surface.

A further effect of the serrations is the streaked, relative high and low speed flow immediately downstream. The effects of this are twofold, firstly this assists with the dampening of turbulence present in the incoming flow which is beneficial in noise reduction and the serrations in effect can be described as a passive flow straightener [22]. Secondly the streaks increase the energy within the boundary layer which delays separation, particularly at higher AoA, thus improving lifting performance and a potential noise reduction [1, 23]. It is important to note however that these streaks are none vorticial and the serrations themselves do not shed vorticies [22] as would be the case in other swept wing flow control devices.

2. Variation with AoA

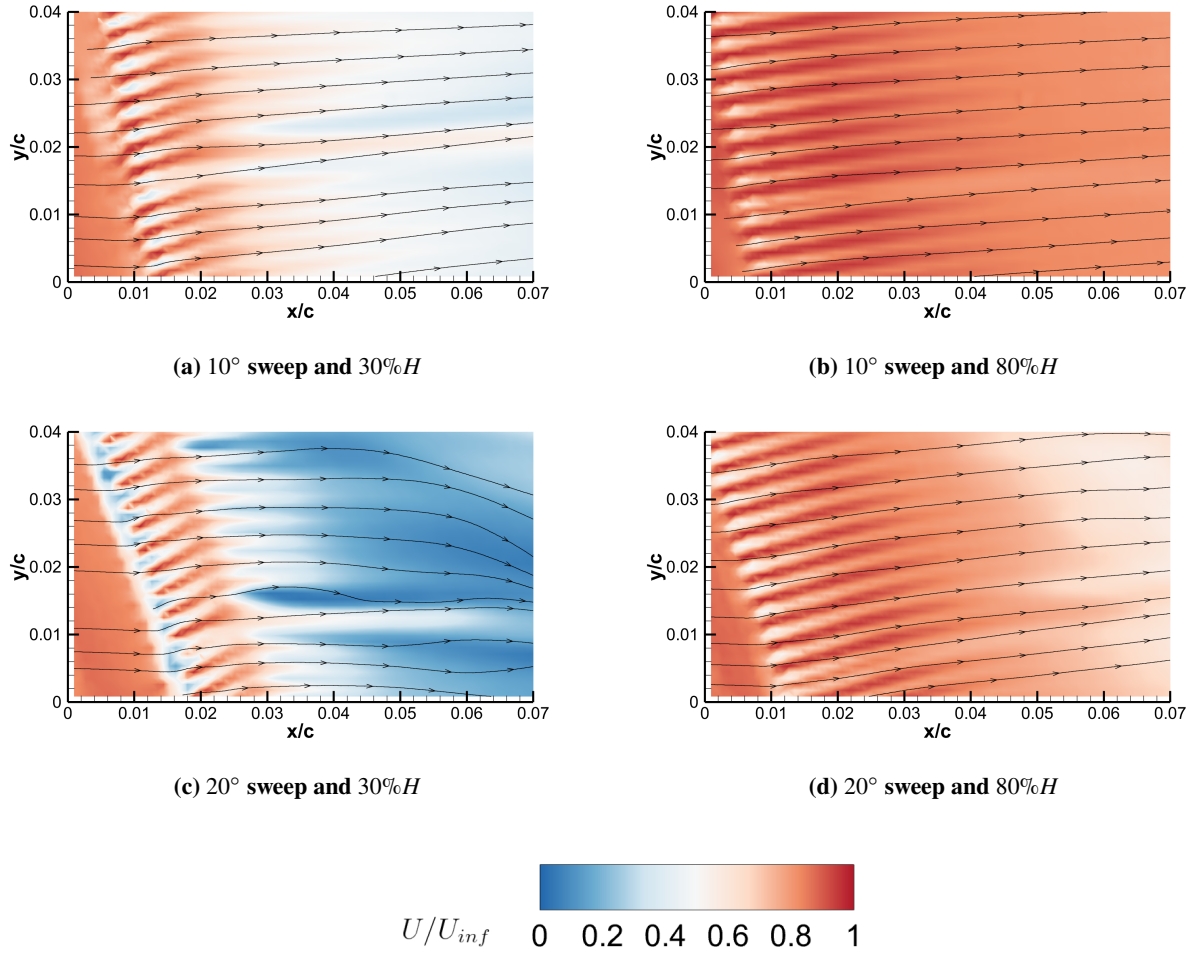

(a) 10° **sweep and** 30%H

(b) 10° **sweep and** 80%H

(c) 20° **sweep and** 30%H

(d) 20° **sweep and** 80%H

Fig. 6 Serration reference case velocity magnitude contours with overlaid streamlines at 10° **AoA and** $Re_s = 80,000$ **at different sweep angles.**

Similar to the reference case the flow turning is dependent primarily on the height of the barbs where the measurement is taken. However more interesting effects occur with the increase in AoA and subsequent change in streamwise cross

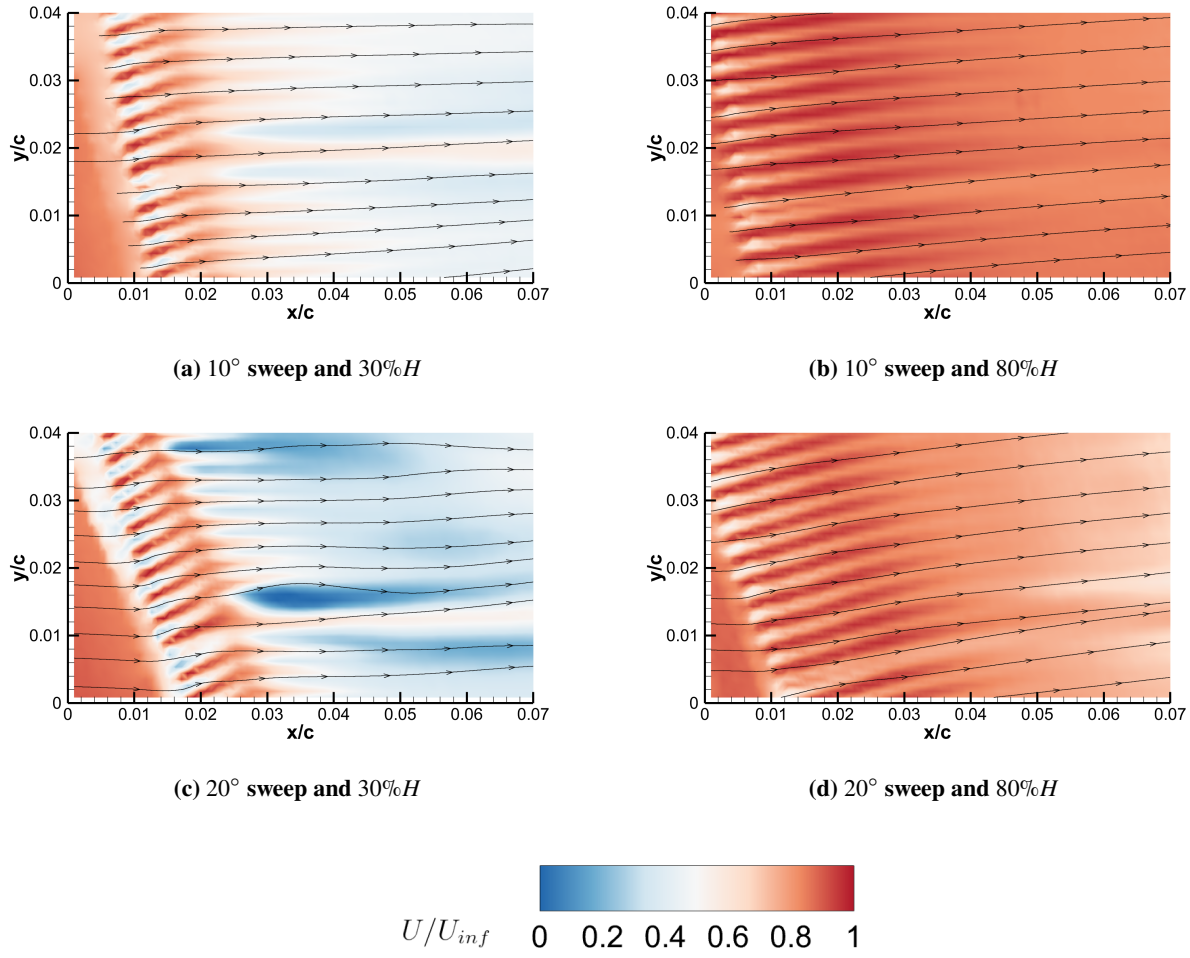

(a) 10° **sweep and** 30%H

(b) 10° **sweep and** 80%H

(c) 20° **sweep and** 30%H

(d) 20° **sweep and** 80%H

Fig. 7 Serration reference case velocity magnitude contours with overlaid streamlines at 20° **AoA and** $Re_s = 80,000$ **at different sweep angles.**

sectional area at a given height. Figures 6 and 7 show the variation in flow turning with respect to angle of attack. At the 30%H serration heights flow is turned inboard less with increased angle of attack (indicated by the streamlines becoming more horizontal). However at 80%H the flow turning remains consistent regardless of AoA for both sweep cases.

Figure 8 shows the variation of the flow turning effect dependent on the AoA and percentage serration height. Across the range of AoA the flow turning at 80%H remains consistent for each respective sweep angle. However as the incident angle of the incoming flow with respect to the barb orientation is greater with 20° sweep the resulting flow turning at the higher percentage H is also slightly larger (view fig. 3). However at the lower, 30%H the amount of flow turning is heavily dependent on the AoA and at both sweep angles the variation is ≈4°.

The variation in flow turning angle at the lower serration height in both cases can be approximated by a third order polynomial and follow a similar regression with increased AoA. Interestingly with $\beta = 10°$ the serrations have a greater effective range of flow turning and a higher peak value of 7° but, they are less effective than with 20° of sweep beyond 20° AoA. This is consistent with the flight profile (change in AoA and sweep angle) of an owl during the flaring maneuver in which the sweep and AoA increase but flow attachment and noise suppression needs to be maintained in the final moments of flight.

Across the AoA range tested a reversal of the flow turning direction (towards the tip) was not observed as was seen by Anderson ([5]). There are a number of causes that could lead to this discrepancy:

1) The model used herein is a idealized version of an owls serrations so may not fully capture the natural geometry

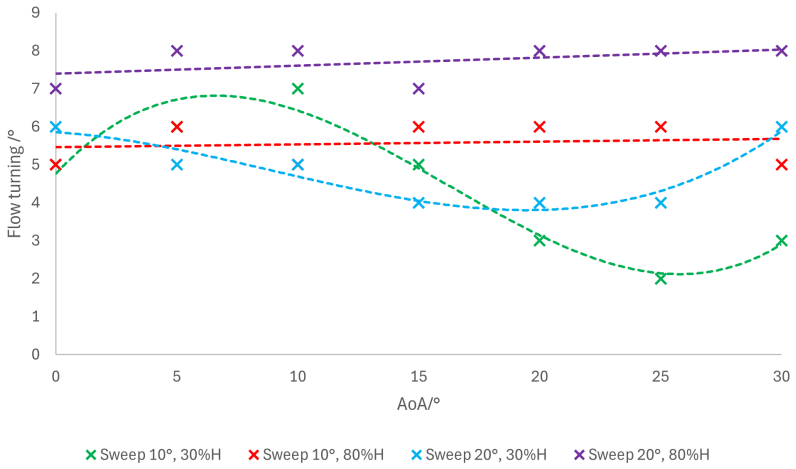

Fig. 8 Variation of the inboard flow turning effect of owl serrations witch changes in AoA and sweep.

which could reverse the flow from inboard to outboard in certain conditions.

2) Also only two cross sections of the serrations were analyzed, with the lowest measurement plane at 30%H. As can be seen in fig. 8, and particularly at the $\beta = 10°$, the flow turning drastically reduces with increased angle of attack so could be turned towards the tip at the serration root.
3) Lastly other features of found on an owls wing which may contribute further to the reversal of the flow turning are not present in this study.

B. Modification of the tip vortex

Figure 9 shows the development of the tip vortex downstream for the 10° sweep wings with and without serrations attached. The core size can be seen to be reduced marginally when the serrations are attached to the leading edge. This is due to the flow turning countering the natural outboard flow found on swept wings that eventually roll up into the tip vortex. In this regard the serrations can be compared to swept wing flow control devices (namely vortex generating jets and wing fences [13]), not only in their ability to delay separation [23] but also inclined streaked flow acts as an obstruction to the spanwise velocity component.

The reduction in core size may explain the findings of [9, 10] that the flight noise production of an owl wing was lower with the leading edge serrations attached. A smaller vortex core size relates in general to a reduced noise emission in vortex-induced sound [24]. The addition of the serrations on the leading edge also does not modify the location of the vortex (slightly above the wingtip and inboard in each case fig. 9). This remained consistent where a vortex was distinguishable in the other test cases (before the airfoil fully stalled)[25].

VII. Conclusion

Serrations have been demonstrated to be a passive flow control device which affects the near-wall flow over the wing and consequently also the roll-up of the tip vortex, dependent on the AoA and sweep of a wing. The complex curvature and twist of the serrations induces flow turning that changes in magnitude and direction depending on the height of the barbs and the inflow conditions. For swept wings, the flow turning reduces the spanwise velocity component in the boundarly layer considerably and consequently also the spanwise shear layer which is contributing to the vorticity roll-up into the tip vortex. This would suggest that the serrations work in a similar way to other swept wing flow control devices by reducing the spanwise flow, already shown to delay separation [23]. Further, the documented reduction in tip vortex core size and strength with attached leading edge serrations would indicate a reduction in noise emission ([24]). This adds to another function of the serrations that enable an owl's silent flight, by reducing the tip-vortex strength particularly in the final flare during hunting.

Future research on the effects of serrations on swept wings should assess the changes to the aerodynamic performance, particularly in relation to other passive and active flow control devices. Potential optimization of the serrations could also be reviewed, specifically in relation to λ and the number of serrations/ their placement along the wing span.

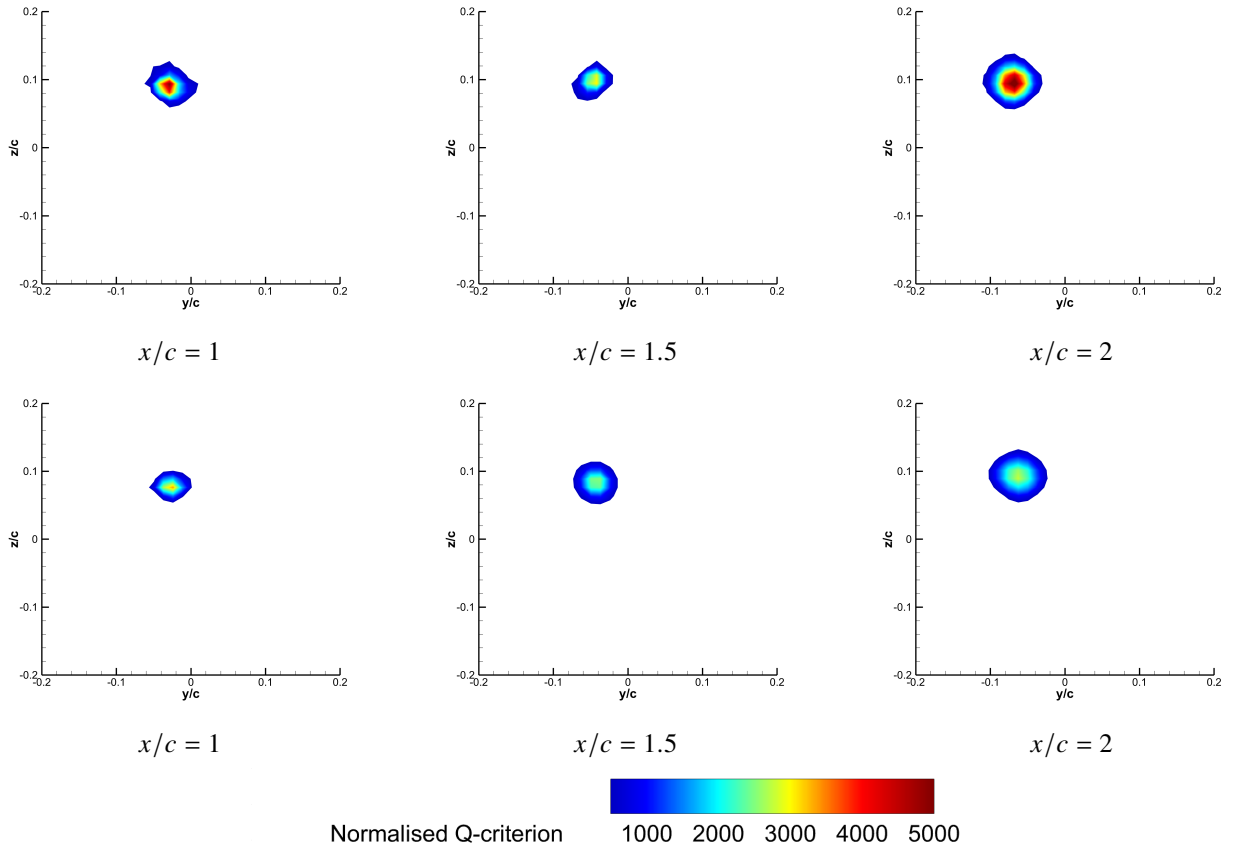

Fig. 9 Q-criterion of the vortices produced by the $\beta = 10°$ wings at $\alpha = 10°$ without serrations (top row) and with serrations attached (bottom row).

Acknowledgments

The position of Professor Christoph Bruecker is co-funded as the BAE SYSTEMS Sir Richard Olver Chair and the Royal Academy of Engineering Chair (grant RCSRF1617/4/11) which is gratefully acknowledged. Alden Midmer is co-funded by City, University of London and BAE SYSTEMS which is gratefully acknowledged.

References

[1] Graham, R., "The silent flight of owls JR Aeronaut," *Soc*, Vol. 286, 1934, pp. 837–843.

[2] Jaworski, W., and Peake, N., "Aeroacoustics of silent owl flight," *Annual Review of Fluid Mechanics*, Vol. 52, 2020, pp. 395–420.

[3] Geyer, T., V, C., P, H., and E, S., "Silent owl flight: the effect of the leading edge comb," *International Journal of Aeroacoustics*, Vol. 16, No. 3, 2017, pp. 115–134.

[4] Rao, C., T, I., T, N., and H, L., "Owl-inspired leading-edge serrations play a crucial role in aerodynamic force production and sound suppression," *Bioinspiration & biomimetics*, Vol. 12, No. 4, 2017, p. 046008.

[5] Anderson, G. W., "An experimental investigation of a high lift device on the owl wing," Ph.D. thesis, Air Force Institute of Technology, 1973.

[6] Kroeger, R., H, G., T, H., et al., *Low speed aerodynamics for ultra-quiet flight*, Air Force Flight Dynamics Laboratory, Air Force Systems Command, United States Air Force, 1972.

[7] Neuhaus, W., H, B., and B, S., "Morphologische und funktionelle Untersuchungen über den'lautlosen'Flug der Eulen (Strix aluco) im Vergleich zum Flug der Enten (Anas platyrhynchos)," *Biologisches Zentralblatt*, Vol. 92, 1973, pp. 495–512.

[8] Sarradj, E., C, F., and T, G., "Silent owl flight: bird flyover noise measurements," *AIAA journal*, Vol. 49, No. 4, 2011, pp. 769–779.

[9] Geyer, T., E, S., and C, F., "Measuring owl flight noise," *INTER-NOISE and NOISE-CON Congress and Conference Proceedings*, Vol. 249, Institute of Noise Control Engineering, 2014, pp. 183–198.

[10] Geyer, T., V, C., and E, S., "Silent owl flight: The effect of the leading edge comb on the gliding flight noise," *22nd AIAA/CEAS Aeroacoustics Conference*, 2016, p. 3017.

[11] Philipp, T., Roman, S., Emilio, G., and Israel, W., "IL01 CONTROL OF SEPARATION ON SWEPT BACK WINGS IN VIEW OF THE BOUNDARY LAYER INDEPENDENCE PRINCIPLE," *The Proceedings of the International Conference on Jets, Wakes and Separated Flows (ICJWSF) 2013.4*, The Japan Society of Mechanical Engineers, 2013, pp. _IL01–1_.

[12] Walker, M. M., and Bons, J. P., "The effect of passive and active boundary-layer fences on swept-wing performance at low Reynolds number," *2018 AIAA Aerospace Sciences Meeting*, 2018, p. 0793.

[13] McFadden, E. J., Brandt, P. J., and Bons, J. P., "Swept-Wing Active Flow Control with a Streamwise Row of Vortex Generating Jets," *AIAA Journal*, Vol. 61, No. 3, 2023, pp. 1142–1150.

[14] Muthuramalingam, M., Talboys, E., Wagner, H., and Brücker, C., "Flow turning effect and laminar control by the 3D curvature of leading edge serrations from owl wing." *Bioinspiration and Biomimetics*, Vol. 16, 2020.

[15] Bachmann, T., "Anatomical, morphometrical and biomechanical studies of barn owls' and pigeons' wings," Ph.D. thesis, Aachen, Techn. Hochsch., Diss., 2010, 2010.

[16] Wagner, H., and PM, P., "A Comparison of Aerodynamic Parameters in Two Subspecies of the American Barn Owl (Tyto furcata)," *Animals*, Vol. 12, No. 19, 2022, p. 2532.

[17] Bachmann, T., and H, W., "The three-dimensional shape of serrations at barn owl wings: towards a typical natural serration as a role model for biomimetic applications," *Journal of anatomy*, Vol. 219, No. 2, 2011, pp. 192–202.

[18] Zierep, J., *Ähnlichkeitsgesetze und Modellregeln der Strömungslehre*, Springer-Verlag, 2013.

[19] Raffel, M., C, W., F, S., C, K., and J, W. S. K., *Particle image velocimetry: a practical guide*, Springer, 2018.

[20] Wagner, H., M., W., M., K., and W., S., "Features of owl wings that promote silent flight," *Interface focus*, Vol. 7, No. 1, 2017, p. 20160078.

[21] Thielicke, W., and E.J, S., "PIVlab Towards User-friendly, Affordable and Accurate Digital Particle Image Velocimetry in MATLAB." *Journal of Open Research Software*, Vol. 2(1):e30, 2014. https://doi.org/http://dx.doi.org/10.5334/jors.bl.

[22] Midmer, A., Brücker, C., Weger, M., Wagner, H., and Bleckmann, H., "Interaction of barn owl leading edge serrations with freestream turbulence," *Bioinspiration & Biomimetics*, Vol. 19, No. 3, 2024, p. 036014.

[23] Saussaman, T., A, N., D, C., H, B., and R, G., "The role of leading-edge serrations in controlling the flow over owls' wing," *Bioinspiration & Biomimetics*, 2023.

[24] Klei, C., R.M., B., and E., S., "Effects of wing tip shaping on noise generation," *INTER-NOISE and NOISE-CON Congress and Conference Proceedings*, Vol. 249, Institute of Noise Control Engineering, 2014, pp. 1984–1993.

[25] Gerontakos, P., and Lee, T., "Near-field tip vortex behind a swept wing model," *Experiments in Fluids*, Vol. 40, 2006, pp. 141–155.